Original

Knaapila, M.; Evans, R.C.; Gutacker, A.; Haramus, V.M.; Szekely, N.K.; Scherf, U.; Burrows, H.D.:

Conjugated polyelectrolyte (CPE) poly[3-[6-(N-methylimidazolium)hexyl]-2,5-thiophene] complexed with aqueous sodium dodecylsulfate amphiphile: synthesis, solution structure and "surfactochromic" properties

In: Soft Matter (2011) RSC Publishing

DOI: 10.1039/C1SM05492A

Soft Matter

View Online
Dynamic Article Links

Cite this: *Soft Matter*, 2011, **7**, 6863

www.rsc.org/softmatter

PAPER

Conjugated polyelectrolyte (CPE) poly[3-[6-(*N*-methylimidazolium)hexyl]-2,5-thiophene] complexed with aqueous sodium dodecylsulfate amphiphile: synthesis, solution structure and "surfactochromic" properties†

Matti Knaapila,*[a] Rachel C. Evans,[b] Andrea Gutacker,[c] Vasil M. Garamus,[d] Noémi K. Székely,[e] Ullrich Scherf[c] and Hugh D. Burrows[f]

Received 22nd March 2011, Accepted 11th May 2011
DOI: 10.1039/c1sm05492a

We report on the synthesis, solution structure and photophysical properties of poly[3-[6-(*N*-methylimidazolium)hexyl]-2,5-thiophene] bromide (P3ImiHT) when complexed with sodium dodecylsulfate (SDS). Synthesis of P3ImiHT used a Grignard metathesis (GRIM)-type route developed by McCullough, followed by quaternisation of the bromohexyl side groups of poly[3-(6-bromohexyl)-thiophene] with *N*-methylimidazole. P3ImiHT was mixed with either SDS or deuterated SDS to form the P3ImiHT(SDS)$_x$ complex, where x is the molar ratio of surfactant to polyelectrolyte repeat unit, in D_2O and studied using small-angle neutron scattering (SANS) and optical spectroscopy. Marked differences in behaviour are observed upon interaction of P3ImiHT with SDS compared with the related poly[3-(6-trimethylammoniumhexyl)thiophene] bromide (P3TMAHT). At room temperature, P3ImiHT forms charged aggregates with electrostatic repulsion which are eliminated by the SDS addition. For $x \leq 1$ P3ImiHT and SDS are molecularly mixed and form ellipsoidal ($x = 1/5$) or sheet-like ($x = 1/2$–1) P3ImiHT(SDS)$_x$ aggregates. No visible precipitation is observed around the nominal charge compensation point ($x = 1$). For $x > 1$, P3ImiHT(SDS)$_x$ aggregates coexist with SDS rich micelles which turn from thick rod-like ($x = 3/2$) to non-charged ($x = 2$) and charged ellipsoidal micelles ($x = 5$). This transition is driven by decreasing free ion fraction. For $x = 5$, P3ImiHT(SDS)$_x$ forms a lamellar phase with a periodicity of ~270 Å. The structural transitions are accompanied by an initial red-shift from 422 nm ($x = 0$) to 459 nm ($x = 1$), followed by a reverse blue-shift to 400 nm ($x = 5$) of the UV/vis absorption maxima. The photoexcitation spectra follow this trend but are ~50 nm red-shifted, thus indicating energy transfer within the density of states after photoexcitation. The photoluminescence maximum is gradually blue-shifted from 643 nm to 597 nm on increasing x from 0 to 5, indicating a decrease in polymer–polymer interactions.

Introduction

Water soluble π-conjugated polymers[1] have been employed in myriad processing techniques such as inkjet,[2,3] layer-by-layer[4,5] and Langmuir–Blodgett[6–8] processes. They show potential in many applications such as light emitting diodes,[9,10] chemosensors[11,12] and biosensors,[13–16] where water provides a harmless media for device environment or signal amplification.

Water solubility can be achieved by means of π-conjugated polyelectrolytes (CPEs),[17] which typically involves incorporating hydrophilic terminal groups such as non-charged ethynylene[18] or charged amino groups[19–21] into side chains off the polymer backbone. CPEs can also act as ionic liquids,[22–24] dissolving water in small polymer fractions and self-assembling into supramolecular structures in higher fractions, much of this behaviour being attributed to their "hairy-rod" type structure.[25] Another possibility is the combination of two ionomers which is best known for poly(3,4-ethylenedioxythiophene) with poly(4-styrenesulfonate).[26] Supramolecular charge-transfer complexes combining several π-conjugated oligomers have also been investigated in water.[27]

Solubility can also be attained by the addition of non-ionic surfactants,[28–31] which may form a layer between the polymer

[a]*Physics Department, Institute for Energy Technology, NO-2027 Kjeller, Norway. E-mail: matti.knaapila@ife.no*
[b]*School of Chemistry, Trinity College Dublin, Dublin 2, Ireland*
[c]*Fachbereich Chemie, Bergische Universität Wuppertal, D-42097 Wuppertal, Germany*
[d]*Helmholtz-Zentrum Geesthacht: Zentrum für Material- und Küstenforschung GmbH, D-21502 Geesthacht, Germany*
[e]*BNC, Research Institute for Solid State Physics and Optics, H-1525 Budapest, Hungary*
[f]*Departamento de Química, Universidade de Coimbra, 3004-535 Coimbra, Portugal*

† Electronic supplementary information (ESI) available: Details of polymer synthesis and NMR data. Photoluminescence (PL) spectra with $\lambda_{ex} = 500$ nm. Photoexcitation spectra with $\lambda_{em} = 680$ nm. UV/vis, PL and photoexcitation spectra after 1000-fold dilution. See DOI: 10.1039/c1sm05492a

and water.[30] This strategy is seemingly beneficial since the polymer solubility can be manipulated simply by varying the surfactant fraction, therefore eliminating the need to synthesise a series of polymers. Surfactant addition may also cause a variation in the optical properties, leading to effects such as spectral shifts, so called surfactochromism,[31] and fluorescence enhancement.[28] The surfactant presence can also improve both sensitivity and selectivity in biosensing applications.[13,29]

It is also possible to tailor solubility by adding bulky counterions or ionic surfactants, which act effectively as counterions for CPEs, as pioneered by McCullough,[32,33] Whitten[34] and others. Increasing the counterion size can lead to significant spectral shifts, for example, from a red aggregated phase to a yellow solution with disrupted polythiophene aggregates.[32,33] This effect is akin to the order–disorder transition from an ordered solid of rigid rods to a disordered liquid of more coiled polythiophene chains.[35,36]

Non-ionic π-conjugated polymers can also be covalently bonded to polyelectrolytes providing a route to water-soluble block copolymers.[37] A series of water soluble all π-conjugated block copolymers have been introduced by Scherf *et al.*,[38] including one example, where a hydrophobic poly(9,9-dioctylfluorene) (PFO) block is coupled to a polyelectrolytic poly[3-(6-trimethylammoniumhexyl)thiophene] (P3TMAHT) block to form the block copolymer PFO-*b*-P3TMAHT.[39] Addition of an oppositely charged surfactant such as sodium dodecylsulfate (SDS) to its aqueous solution leads to significant changes in the small-angle scattering data together with photoluminescence (PL) enhancement indicating the occurrence of multifarious surfactant-induced structural changes. Indeed, the combination of the two polymer blocks in PFO-*b*-P3TMAHT, both differing in their solubility and electronic properties, results in a single material offering a richness of behaviour in terms of both its optical and structural characteristics. However, to fully understand and exploit the factors pertaining to the structural reorganisation of PFO-*b*-P3TMAHT and related block copolymers, the behaviour of the isolated charged polythiophene is a much better starting point for our studies.

To this end we recently performed a structural and photophysical study of the interactions of P3TMAHT upon SDS addition in water and observed formation of the P3TMAHT $(SDS)_x$ complex, where x is the molar ratio of surfactant over monomer units.[40] At room temperature P3TMAHT shows a series of structural transitions with increasing SDS fraction, which may be visibly followed by distinctive changes in the solution colour from red to violet and yellow. While providing a good example in terms of surfactochromism, partial precipitation occurs at the charge compensation point ($x = 1$).

In order to minimise this precipitation tendency and to produce processable materials with potential optoelectronic applications, we turn to poly[3-[6-(*N*-methylimidazolium)hexyl]-2,5-thiophene] (P3ImiHT). P3ImiHT differs from P3MAHT only in the identity of its cationic side-chain: the trimethylammonium group of P3MAHT is now substituted for *N*-methylimidazole. The *N*-methylimidazole substituent is expected to result in improved shielding of the ionic centre in polymer.

This polymer class has scarcely been studied, a recent report of Bondarev *et al.*[41] representing an exception. A related polymer with *N*-(methylimidazolium)decyl side chains has also been synthesised by Firestone *et al.*,[22,23] who found it formed well-dissolved coils in dilute aqueous solution and columnar structures at high (20–40 w/w) polymer fractions.

In this paper we mix P3ImiHT with SDS to form P3ImiHT $(SDS)_x$ and study this complex using neutron scattering and optical spectroscopy in D_2O solutions. We suggest that at room temperature P3ImiHT forms charged aggregates with interparticle order. Addition of SDS eliminates the interparticle order and leads to a sequence of ellipsoidal ($x = 1/5$) and sheet-like polymer–SDS aggregates ($x = 1/2$–1) with increasing x. Within the polymer–surfactant aggregates, the polymer organisation follows the shapes of the overall complex for $x = 1/5$ and 1, but becomes laterally well-ordered for $x = 5$. P3ImiHT$(SDS)_x$ aggregates coexist with SDS rich micelles for $x > 1$. The structural variation is followed by "surfactochromic" effects including a red-shift and a subsequent reverse blue-shift in the photoabsorption spectra when increasing x around the nominal charge compensation point ($x = 1$). In contrast to the previously studied P3TMAHT, visual precipitation at the charge-compensation point ($x = 1$) is not observed and vibronic structure is predominantly absent in both the absorption and emission spectra. These results shed light on the phase behaviour of the P3ImiHT complexed with oppositely charged surfactant, a system where the optical transitions are induced by changes in the polymer conformation *within* polymer–surfactant aggregates, and provide a structure that can be controlled simply by varying the surfactant fraction. This work contributes to the general understanding of structural interactions and phase behaviour in water soluble polythiophenes and can also help in understanding the analogous block copolymers.

Experimental section

Materials

The synthetic route towards P3ImiHT is shown in Fig. 1a. First, 3-bromothiophene and 1,6-dibromohexane are coupled to 3-(6-bromohexyl)thiophene. This is followed by bromination of 3-(6-bromohexyl)thiophene with *N*-bromosuccinimide (NBS) to obtain 2-bromo-3-(6-bromohexyl)thiophene, which is subsequently polymerised in a Grignard metathesis (GRIM) procedure to yield poly[3-(6-bromohexyl)thiophene] (P3BrHT) as previously described by McCullough and Zhai.[5] The final step to the target polyelectrolyte P3ImiHT is a polymer-analogous quaternisation of the bromohexyl side groups with *N*-methylimidazole.

GPC analysis of the P3BrHT precursor displayed a mean average molecular weight M_n of *ca.* 5000 g mol^{-1} and a weight average M_w of *ca.* 7000 g mol^{-1} (degree of polymerisation *ca.* 20). We could not exactly measure the molecular weight of the cationic polyelectrolyte P3ImiHT by GPC due to the strong interaction of the polyelectrolyte with the column. The NMR data of P3ImiHT are in accordance with the proposed chemical structure (see ESI†).

SDS (Fig. 1b) was purchased from Sigma-Aldrich and deuterated SDS (SDS-d_{25}) (98.5% D) from CND Isotopes. These materials were mixed with D_2O (99.9% D, Cambridge Isotope Laboratories Inc). P3ImiHT$(SDS)_x$–D_2O mixtures, where x stands for the molar ratio of SDS over P3ImiHT monomers,

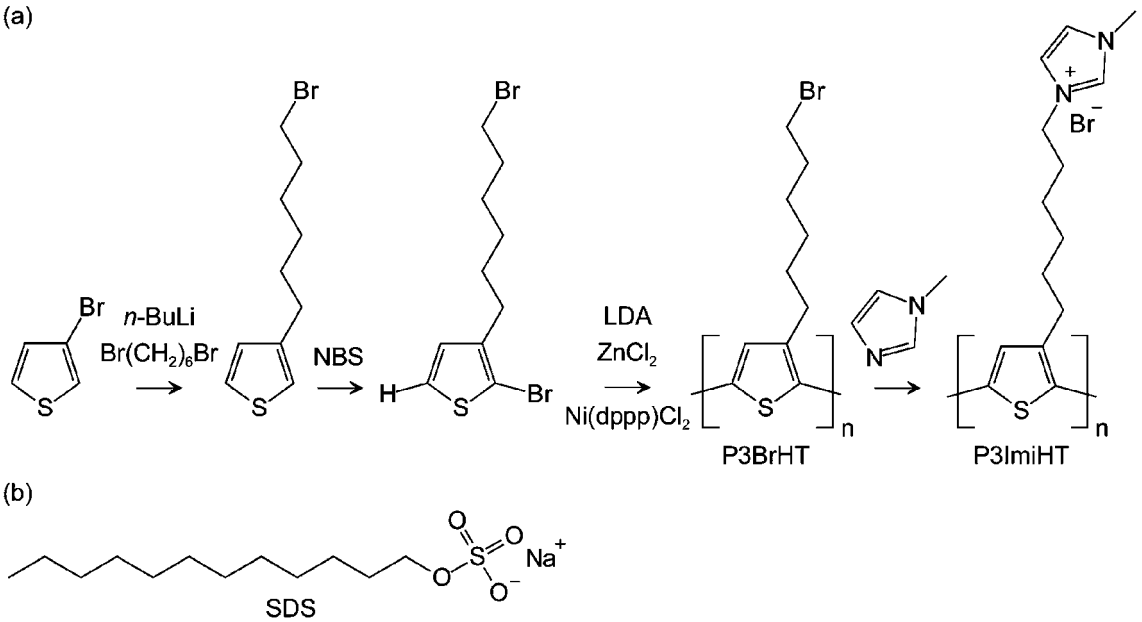

Fig. 1 (a) Synthetic route towards the polyelectrolyte P3ImiHT. (b) Chemical structure of SDS surfactant.

were prepared by mixing 10 mg mL^{-1} P3ImiHT–D_2O solution, with the concentration given with respect to the P3ImiHT monomer unit, with 10.35 mg mL^{-1} SDS–D_2O solution so that the desired molar ratio x was reached. The value $x = 1$ corresponds to the stoichiometric charge balance. The compositions of polymer–surfactant complexes are given in Table 1.

Instrumentation and methods

Photographs of the samples were taken using a Canon Ixus digital camera.

Some SANS measurements of P3ImiHT, SDS, and P3ImiHT $(SDS)_x$–D_2O were performed on the *Yellow Submarine* instrument at the BNC in Budapest (Hungary).[42] Further SANS measurements of P3ImiHT$(SDS)_x$–D_2O and all SANS measurements of P3ImiHT$(SDS\text{-}d_{25})_x$–D_2O were performed at the SANS-1 instrument at the Helmholtz-Zentrum Geesthacht (Germany).[43] The overall q-range was from 0.01 to 0.27 Å^{-1}. In all cases the samples were filled in Hellma quartz cells of 2 mm path length and placed in a thermostated holder at 20.0 ± 0.5 °C.

Table 1 Composition of P3ImiHT$(SDS)_x$–D_2O and P3ImiHT$(SDS\text{-}d_{25})_x$–D_2O samples

x	Monomer conc./mg mL^{-1}	SDS conc./mg mL^{-1}	SDS-d_{25} conc./mg mL^{-1}	Overall conc./mg mL^{-1}
0	10.00			10.00
1/5	8.33	1.73		10.06
1/5	8.33		1.74	10.08
1/2	6.67	3.45		10.12
2/3	6.00	4.14		10.14
1	5.00	5.18		10.18
1	5.00		5.23	10.23
3/2	4.00	6.21		10.21
2	3.33	6.90		10.23
5	1.67	8.63		10.29
5	1.67		8.71	10.38

The raw scattering patterns were corrected for sample transmission, room background, and sample cell scattering. The 2-dimensional scattering patterns were azimuthally averaged, converted to an absolute scale and corrected for detector efficiency by dividing by the incoherent scattering spectra of 1 mm thick pure water. The scattering from a mixture of D_2O and water (99 : 1) was subtracted as the background.

The scattering functions were interpreted using scaling concepts. Here we considered the scattering intensity as

$$\frac{1}{c}\frac{\mathrm{d}\sum(q)}{\mathrm{d}\Omega} \sim q^{-\alpha} \quad (1)$$

where c is the concentration and the exponent $\alpha = 1$ refers to separated rod-like or cylindrical particles and $\alpha = 2$ to sheet-like particles. Smooth 3-dimensional particles would show an exponent $\alpha = 4$ and the scattering would level off at low scattering angles. This first interpretation was enhanced by numerical modeling to the assumed geometric shapes using the indirect Fourier transformation (IFT) program GNOM.[44] This analysis gives an idea of possible particle shapes and sizes. However, it does not take polydispersity into account.

UV/vis absorption spectra were recorded on a Shimadzu UV-2100 spectrometer at room temperature. The measurements were performed on the same samples used for scattering measurements to enable direct comparison. To overcome the problem of a saturated signal and self-absorption the samples were prepared by sandwiching a small volume (6 μL) of P3ImiHT$(SDS)_x$–D_2O between two glass microscope cover slips. Spectra were background corrected for the absorption of the cover slips and the solvent. Three measurements were performed to ensure reproducibility. Attenuation of the reference beam was made for the sample with the lowest polymer concentration ($x = 5$) using an in-built neutral density filter (1% T).

Photoluminescence (PL) measurements were performed using a HORIBA Jobin Yvon Fluorolog-3 fluorimeter in front face geometry at room temperature. The samples were measured in

Fig. 2 A photograph of P3ImiHT(SDS)$_x$–D$_2$O samples for $x = 0$ (left), $x = 1$ (middle), and $x = 5$ (right) at room temperature.

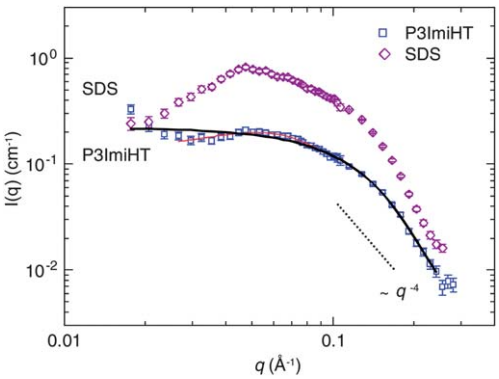

Fig. 3 SANS data of P3ImiHT–D$_2$O (open blue squares). The data of SDS–D$_2$O (open purple diamonds) are shown for comparison. The solid black line shows a model fit and the solid red line is a fit to the interference maximum as described in the text. The dotted line shows a −4 slope for comparison. The overall concentration was ~10 mg mL^{-1}, $T = 20$ °C.

quartz cuvettes with a short path length (1 mm). Excitation and emission monochromator slit widths were both maintained at 2.5 nm for all samples. Spectra were corrected for the wavelength response of the system using correction factors supplied by the manufacturer.

For comparison the P3ImiHT(SDS)$_x$–D$_2$O samples were diluted to ~0.01 mg mL^{-1} in water. UV/vis absorption spectra and PL and excitation spectra were recorded on the same instruments as above in a 1 cm path length quartz cuvette.

Results and discussion

Polymer synthesis

As already discussed in the Materials section, Fig. 1a depicts the synthetic route to the target polyelectrolyte P3ImiHT. Its NMR data are in agreement with the proposed structure and are included in the ESI†. The synthesis of P3ImiHT has previously been reported by Bondarev *et al.*[41] However, our synthetic procedure, and more specifically, our quaternisation process involving the reaction of bromohexyl side groups with *N*-methylimidazole, differs from the previously described route.[41]

Visual considerations

Fig. 2 shows a photograph of P3ImiHT(SDS)$_x$–D$_2$O as a function of molar ratio x. In the solid state P3ImiHT powder appears visually red and the colour is not changed on dissolution in D$_2$O. The solution becomes gradually orange on SDS addition at concentrations around the nominal charge compensation point (*i.e.*, when $x = 1$) and subsequently turns yellow for higher x. Similar, but not identical, colour changes are reported for HT-2,5-poly(thiophene-3-propionic acid) with increasing counterion size[32,33] and observed for P3TMAHT(SDS)$_x$ with increasing SDS fraction.[40] These previously reported systems, however, show a more purple colour at $x = 1$.

In a previous study, we found that P3TMAHT(SDS)$_x$ forms a system of dissolved and precipitated phases around the charge neutralisation point ($x = 1/2$–1).[40] Similar precipitation has been reported, for instance, for the lysozyme–SDS system.[45] Together lysozyme and oppositely charged SDS form a self-organised complex and at the charge neutralisation point these complexes form a system of dissolved and coexisting precipitated phases. However, no visually apparent precipitation is seen for P3ImiHT–D$_2$O or for any of the studied P3ImiHT(SDS)$_x$–D$_2$O samples. This could be explained in terms of P3ImiHT having a more diffuse charge distribution in the cationic head group than P3TMAHT, which presumably stems from reduced shielding of the ionic centre by the *N*-methylimidazole substituent.

The previously observed visual changes for P3TMAHT(SDS)$_x$–D$_2$O were concomitant with significant structural alterations. To study these variations for P3ImiHT(SDS)$_x$–D$_2$O and to make a comparison to P3TMAHT, we carried out the solution scattering experiments.

Solution structure

Fig. 3 shows SANS patterns of P3ImiHT–D$_2$O and SDS–D$_2$O solutions. The data of P3ImiHT–D$_2$O resemble those of P3TMAHT–D$_2$O[40] and are dominated by an upturn at low q (~0.02 Å^{-1}), a subsequent plateau and a broad interference maximum at higher q (~0.052 Å^{-1}).

A single P3ImiHT chain is rather short, only 80–100 Å, if calculated from the length of the thiophene monomer, which is ~4 Å.[46] This value falls below the upper limit of our observation window (~400 Å) and therefore, if the polymer were dissolved down to the single molecular level, the SANS curve would level off as a Guinier plateau at experimentally attainable q. The emerging plateau suggests separated polymer coils (or rods), whereas an upturn indicates the presence of polymer assemblies. The interference maximum corresponds to a correlation distance of 120 Å and is presumably connected to the interparticle order that stems from electrostatic interactions between charged particles. If the plateau is assumed to determine the local particle size, we obtain a radius of gyration (R_g) of 13.5 ± 0.5 Å (Table 2). These data are in agreement with the small-angle X-ray scattering data of Burns *et al.*[23] who studied a related polythiophene with longer *N*-methylimidazole-terminal alkyl side chains and found an indication of particles (presumed to be polymer coils) with an R_g of 16.9 Å. However we cannot say for sure whether the detected objects contain only one polymer chain. Although the data resemble those of P3TMAHT, the maximum of P3TMAHT is at somewhat lower angles for the corresponding concentration (~0.042 Å^{-1}). A modest upturn at the lowest q

Table 2 Structural parameters obtained from SANS data for P3ImiHT(SDS)$_x$–D$_2$O: α, D_{max}, R_g, $R_{T,g}$, and $R_{CS,g}$, are, respectively, the scattering exponent, considered maximum size of the particle (particle size, sheet thickness or rod diameter) and the radius of gyration for the whole arbitrary-shaped particle, for the thickness of a sheet-like particle or for the cross-section of a cylindrical particle. Maximum refers to the position of an interference maximum

x	Analysed q-range	α	Model	D_{max}/Å	R_g/Å	$R_{T,g}$Å	$R_{CS,g}$/Å	Maximum/Å^{-1}
0	0.018–0.24		Arbit	~40	13.5 ± 0.5			~0.052
1/5	0.018–0.24		Arbit.	~70	18.8 ± 0.8			
2/3	0.018–0.1	2.39 ± 0.04						
	0.018–0.24		Sheet	~15		5.1 ± 0.1		
1/2	0.018–0.1	1.97 ± 0.02						
	0.012–0.25		Sheet	~15		4.9 ± 0.1		
1	0.018–0.1	2.65 ± 0.04						
	0.018–0.24		Sheet	~16		5.1 ± 0.1		
3/2	0.018–0.1	1.36 ± 0.03						
	0.018–0.24		Rod	~37			11.8 ± 0.2	
2	0.012–0.25		Arbit.	~80	23.5 ± 0.33			
5	0.018–0.24							~0.048

implies that samples may experience some degree of aggregate–aggregate overlap. This is, however, not a dominant feature.

Aqueous SDS has a well-known micellar structure[47] and the concentration used here (10.35 mg mL^{-1}) exceeds its critical micelle concentration (~2.4 mg mL^{-1}).[48] The data shown in Fig. 3 are consistent with the well-described SANS data of SDS–D$_2$O[47] with a broad maximum at 0.04–0.05 Å^{-1}; the latter feature stemming from intermicellar interactions. The length of a SDS molecule is 16 Å.

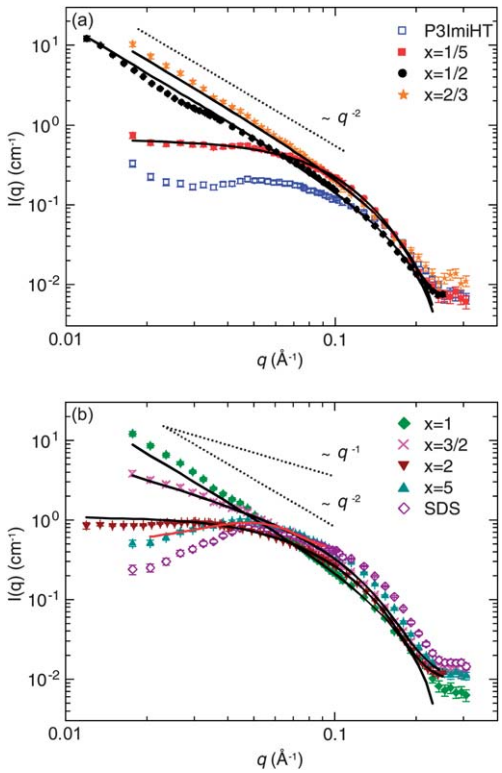

Fig. 4 P3ImiHT(SDS)$_x$–D$_2$O below (a) and above (b) the nominal charge compensation point: x = 1/5 (solid red squares), x = 1/2 (solid black circles), x = 2/3 (solid orange stars), x = 1 (solid green diamonds), x = 3/2 (magenta crosses), x = 2 (solid brown lower triangles) and x = 5 (solid cyan upper triangles). Also shown are SANS data of P3ImiHT–D$_2$O (open blue squares) and SDS–D$_2$O (open purple diamonds) for comparison. The solid black lines represent structural models fitted to the data and the solid red line is a Gaussian fit to the interference maximum for x = 5. Dotted lines show the ideal slopes for comparison. The overall concentration was ~10 mg mL^{-1} for each case, T = 20 °C.

Fig. 4 shows the SANS patterns of P3ImiHT(SDS)$_x$–D$_2$O for x < 1, *i.e.* when the molar ratio is less than the nominal charge compensation point (Fig. 4a), and for $x \geq 1$, *i.e.*, when the ratio equals or exceeds this point (Fig. 4b). The data of P3ImiHT–D$_2$O and SDS–D$_2$O are shown for comparison. The total concentration of all samples is comparable (~10 mg mL^{-1}) and the SDS concentration exceeds its cmc in water in all cases but x = 1/5. Thus, if the surfactant were not complexed, it would form micelles. The SANS data of P3ImiHT(SDS)$_x$–D$_2$O differ significantly from those of P3ImiHT–D$_2$O or SDS–D$_2$O or their superposition, which indicates complexation of oppositely charged moieties and true structural reorganisation.

The scattering intensities follow eqn (1), with the exponent providing an idea of the possible particle shape. Approximate particle sizes were estimated by fitting the data to the appropriate models of the assumed particle shapes using the GNOM software and are depicted by the solid black lines (Fig. 4). Corresponding distance distribution or $p(r)$ functions are shown in Fig. 5. The parameters estimated from these fits are listed in Table 2. No such fits are made for x = 5 due to the observed interference maximum at ~0.048 Å^{-1}. The solid red line is a Gaussian fit to this maximum (Fig. 4b).

The scattering intensities of P3ImiHT(SDS)$_x$–D$_2$O increase on increasing the SDS fraction from x = 0 to x = 1 (Fig. 4a) and decrease on increasing the SDS fraction from x = 1 to x = 5 (Fig. 4b). This behaviour is qualitatively similar to that observed for P3TMAHT[40] and can be interpreted as reaching the point of charge compensation between polymer and surfactant at x = 1. Around this point, the charge balance moderates the polarity and subsequently the water solubility of the material, leading in this case to increased aggregation but not to the precipitation observed for P3TMAHT.[40] We expect that the SDS molecules would not fully compensate the charge of P3ImiHT due to the relative bulkiness of *N*-methylimidazole end groups, in contrast to the trimethylammonium end groups of P3MAHT. Thus the P3ImiHT(SDS) aggregates do not precipitate.

The data for the samples at low SDS fraction (x = 1/5) show a plateau at q < 0.1 Å^{-1}, before decaying as q^{-4} for q > 0.1 Å^{-1}. No interference maxima are observed. These features point to

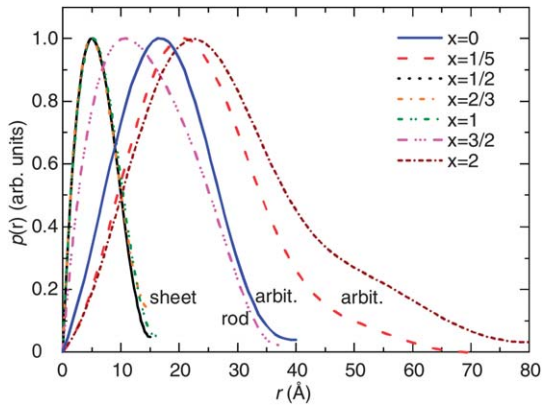

Fig. 5 Examples of distance distribution functions, $p(r)$, as estimated from SANS data of P3ImiHT–D_2O (solid blue line) and P3ImiHT $(SDS)_x$–D_2O for $x = 1/5$ (dashed red line) using an arbitrary shaped particle model; for $x = 1/2$ (dotted black line) and $x = 2/3$ (dashed and dotted orange line) and $x = 1$ (dashed and double dotted green line) using a sheet-like particle model; $x = 3/2$ (dashed and triple dotted magenta line) using a rod-like particle model; and for $x = 2$ (double dashed and dotted brown line) using a model where the particle shape can be arbitrary. These functions correspond to the fits shown in Fig. 3 and 4. The overall concentration of all samples was ~10 mg mL^{-1}.

simple 3-dimensional particles with a smooth surface. The particles are not quite spherical as can be seen from the asymmetric $p(r)$ functions (Fig. 5). SDS is expected to screen electrostatic interactions and must either be incorporated into, or alternatively, absorbed onto the P3ImiHT particles. The screening of electrostatic interactions is also possible due to the release of free bromide ions on the formation of polymer–surfactant aggregates.

Samples with $x = 1/2$–1 show a much higher scattering intensity and this scales approximately as q^{-2}. This behaviour is observed at least for $q < 0.1$ Å^{-1} and is interpreted as the existence of sheet-like particles. The exponent α begins to approach 4 at higher scattering angles, thus marking the thickness of sheet-like particles. The sheets appear large laterally (>400 Å) but simultaneously thin (~20 Å). This thickness corresponds to the solid state d-spacing of poly(3-octylthiophene),[46] which means that the polymer and surfactant must be interwoven rather than forming well-defined layers with respect to each other. In these aggregates SDS is present in its molecular form and not in its supramolecular structures such as spherical micelles, rod-like micelles or bilayers. If the latter case were true, one of the observed dimensions should equal twice the length of SDS molecule (35–40 Å). Similar molecular surfactant complexes have been observed, for example, in solutions of poly(diallyldimethylammonium chloride) and sodium palmitate in the phase regime before the charge compensation point.[49]

Above the charge compensation point, the situation changes, and at $x = 3/2$ the scattering scales as q^{-1}. These data point to rod-like aggregates with a cylindrical cross-section of ~40 Å. This value is higher than the d-spacing of poly(3-octylthiophene)[46] and corresponds to the thickness of surfactant bilayers. We may assume that these rod-like aggregates contain mostly SDS molecules and we may even obtain scattering from pure rod-like SDS micelles at salt excess.

Further increase of the SDS fraction to $x = 2$ leads to a significant decrease in the scattering intensity and the reappearance of the plateau at $q < 0.1$ Å^{-1}. These data approach those of pure SDS micelles, with the remnants of charge screening indicating that the particles are still modified by the polymer. The data for $x = 5$ are very similar to those of pure SDS micelles including the reappearance of the interference maximum, and most of the scattering must originate from the SDS rich micelles.

Fig. 6 shows the SANS patterns of P3ImiHT$(SDS\text{-}d_{25})_x$–D_2O for $x = 1/5$–5. The corresponding data of P3ImiHT$(SDS)_x$–D_2O are also included for comparison. The latter data are from the sample series parallel to those corresponding to the data shown in Fig. 4. The contrast between SDS-d_{25} and D_2O is approximately 50 times lower than that between SDS and D_2O.

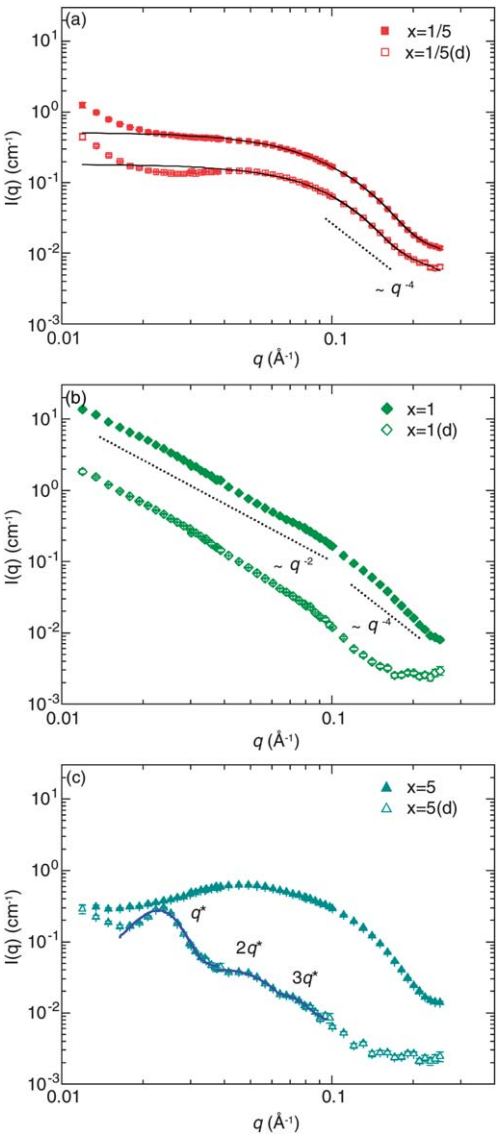

Fig. 6 Comparison of SANS data of P3ImiHT$(SDS\text{-}d_{25})_x$–D_2O and P3ImiHT$(SDS)_x$-D_2O for $x = 1/5$ (a), $x = 1$ (b) and $x = 5$ (c). The open symbols denote the data of samples with SDS-d_{25} and the solid symbols those with SDS. The solid lines represent models fitted to the data (see text for details). Dotted black lines show −2 and −4 decays for comparison, $T = 20$ °C.

Consequently, the contrast difference in the P3ImiHT(SDS-d_{25})$_x$–D_2O system is largest between polymer and D_2O and not between the whole complex and D_2O, meaning that the observed scattering is mainly due to the polymer within P3ImiHT(SDS-d_{25})$_x$ complexes.

In the case of $x = 1/5$ the scattering curve is qualitatively similar to that of the pure polymer (Fig. 3), although the interference maximum is somewhat diminished (Fig. 6a). This means that while the P3ImiHT structure is only moderately influenced by the added SDS in this charge regime, even this small amount may weaken interparticular electrostatic ordering.

In the case of $x = 1$ the scattering curve shows a -2.43 ± 0.02 decay for 0.018–0.1 Å^{-1} thus following the behaviour of P3ImiHT(SDS)$_1$ (Fig. 6b). This points to sheet-like polymer assemblies within sheet-like P3ImiHT(SDS) aggregates. SDS may either be incorporated inside or absorbed onto the aggregates. These data indicate that before and at the charge compensation point, P3ImiHT and SDS form common P3ImiHT(SDS) aggregates and the organisation of P3ImiHT follows the general structure of these aggregates. Any free SDS micelles would only give a minor contribution to the scattering intensity.

The case $x = 5$ is in total contrast, as it shows completely different scattering behaviour from both the P3ImiHT(SDS)$_5$–D_2O complex scattering and the isolated P3ImiHT part of the aggregates. P3ImiHT(SDS)$_5$–D_2O presents smooth scattering of interacting aggregates similar to those of pure SDS micelles, whereas P3ImiHT(SDS-d)$_5$–D_2O shows an interference maximum (q^*) at 0.023 Å^{-1} and putative higher order peaks at 0.045 Å^{-1} ($2q^*$) and 0.063 Å^{-1} ($3q^*$) (Fig. 6c). This clearly indicates the presence of order amongst the polymer, pointing to a loose lamellar phase with a long period of ~270 Å. The origin of these maxima is not clear but may stem from intermolecular order of an emerging self-organised phase, as shown elsewhere for a corresponding polymer with *N*-(methylimidazolium)decyl side chains in dense water solution.[23] We interpret that the order seen in the SANS data for $x = 5$ with SDS-d_{25} originates from different structure to that seen with undeuterated SDS, such that the system must contain ordered P3ImiHT-rich aggregates alongside aggregates that are essentially similar to SDS micelles.

We suppose that the scattering of P3ImiHT(SDS)$_x$–D_2O for $x > 1$ originates mainly from SDS micelles that may be modified by a small amount of polymer. Increasing the SDS fraction x changes the ratio of free ions to the number of SDS molecules in micelles and this leads to the rod-to-sphere transition of SDS-rich micelles when going from $x = 3/2$ to $x = 5$. This phenomenon has been observed for SDS upon addition of amphiphilic salts[50] and analogous behaviour may be anticipated for the 6-(*N*-methylimidazolium)hexyl side chains.

Fig. 7 plots the $p(r)$ functions calculated from the SANS data of P3ImiHT(SDS)$_{1/5}$–D_2O and P3ImiHT(SDS-d_{25})$_{1/5}$–D_2O fitted to the arbitrary-shaped particle model for q = 0.012–0.25 Å^{-1} (Fig. 6a). Important information on the structure is obtained using differences in contrast between normal and deuterated surfactants. The maxima are almost coincident but the data with SDS give a somewhat larger radius of gyration (19.4 ± 0.1 Å) than that with SDS-d_{25} (17.6 ± 0.2 Å). The $p(r)$ function for the SDS data is also more asymmetric than the function observed for SDS-d_{25}. This implies that the P3ImiHT(SDS)$_{1/5}$ aggregates are asymmetric (maximum size ~70 Å) but contain compact, spherical and presumably well packed P3ImiHT particles (maximum size ~50 Å). P3ImiHT appears somewhat larger within the P3ImiHT(SDS)$_{1/5}$ aggregate compared to the free polymer (Table 2). This makes sense assuming that SDS molecules are intertwined with polymer backbone.

Fig. 8 summarises our structural idea of P3ImiHT(SDS)$_x$–D_2O with increasing x with an overall concentration of ~1% at room temperature. P3ImiHT forms charged ellipsoidal particles with supposed electrostatic interactions that are diminished by screening with oppositely charged SDS for $x = 1/5$ and sheet-like aggregates for x = 1/2–1. For $x > 1$ the system consists of two kinds of complexes: P3ImiHT(SDS) aggregates and essentially free SDS micelles. P3ImiHT(SDS) aggregates form a lamellar-like phase with a periodicity of ~270 Å. These structures also incorporate a large volume of D_2O. On increasing x from 3/2 to 5, the SDS micelles change structure from elongated rod-like micelles *via* elliptical micelles to more spherical micelles with increasing electrical charge, due to the decreasing free ion concentration and consequent screening properties of the solution. This picture has similarities to that found for P3TMAHT[40] but the phase region for suggested sheet-like aggregates is narrower and no significant precipitation is observed. This can be plausibly attributed to the better solubility and thus weaker aggregation tendency of P3ImiHT.

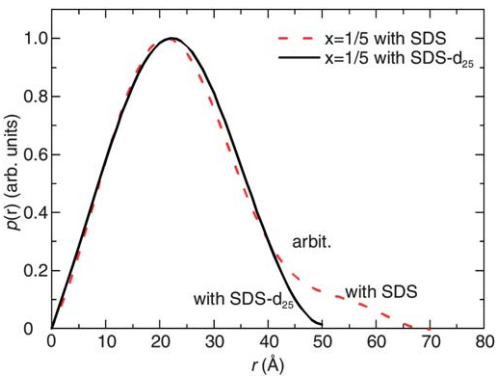

Fig. 7 Distance distribution functions as estimated from the SANS data of P3ImiHT(SDS)$_{1/5}$–D_2O (dashed red line) and P3ImiHT(SDS-d_{25})$_{1/5}$–D_2O (solid black line) using an arbitrary shaped particle model.

Photophysical consequences

Fig. 9 shows UV/visible absorption and PL spectra of P3ImiHT–D_2O and P3ImiHT(SDS)$_x$–D_2O. The photoexcitation wavelength (λ_{ex}) was 450 nm.

The UV/vis spectra are characterised by a broad featureless band for all samples apart from $x = 1/5$, which shows a weak shoulder at the red edge of the absorption band (Fig. 9a). The maximum becomes progressively more red-shifted from 422 nm (for $x = 0$) to 459 nm (for $x = 1$) and a significant, reverse blue-shift is subsequently observed between $x = 1$ and 5. These shifts agree with the observed sample colours from orange/brown (x = 0–1/5) to red/orange (x = 2/3–1), orange/brown ($x = 3/2$) and yellow/orange ($x = 5$) (see examples in Fig. 2). The hump-like low energy features seen for $x = 1/5$ may correspond to P3ImiHT aggregates.

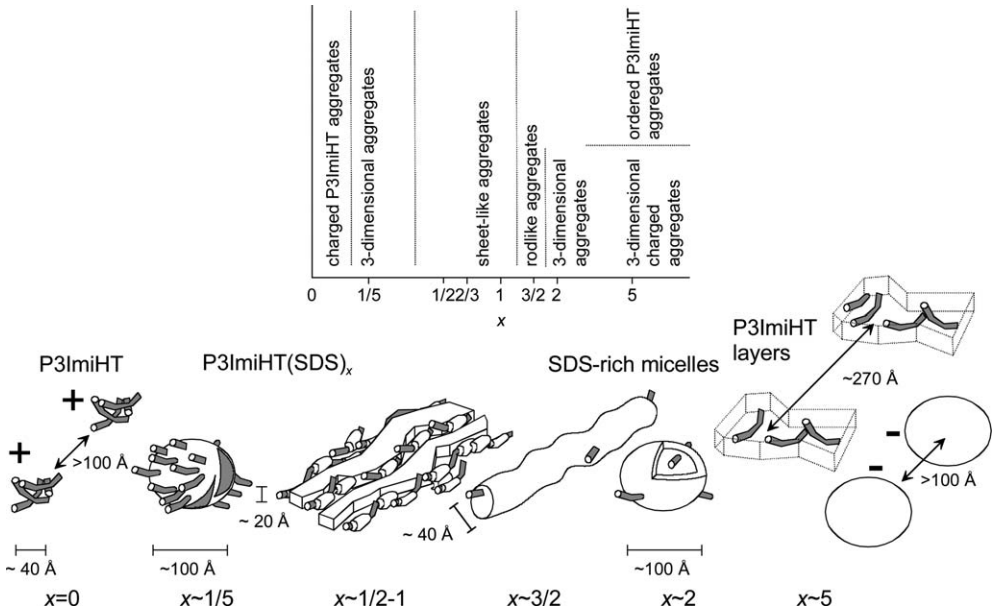

Fig. 8 Top: A phase diagram of P3ImiHT(SDS)$_x$–D$_2$O as a function of x at room temperature, when the overall concentration is ~1%. The dashed lines represent phenomenological phase transitions. Bottom: Illustration of suggested aggregate structures: Charged P3ImiHT aggregates and spherical and sheet-like P3ImiHT(SDS)$_x$ aggregates for $x \leq 1$. Coexisting SDS-rich micelles and P3ImiHT-rich sheets for $x \geq 1$. The gray and white areas refer to P3ImiHT chains and SDS respectively.

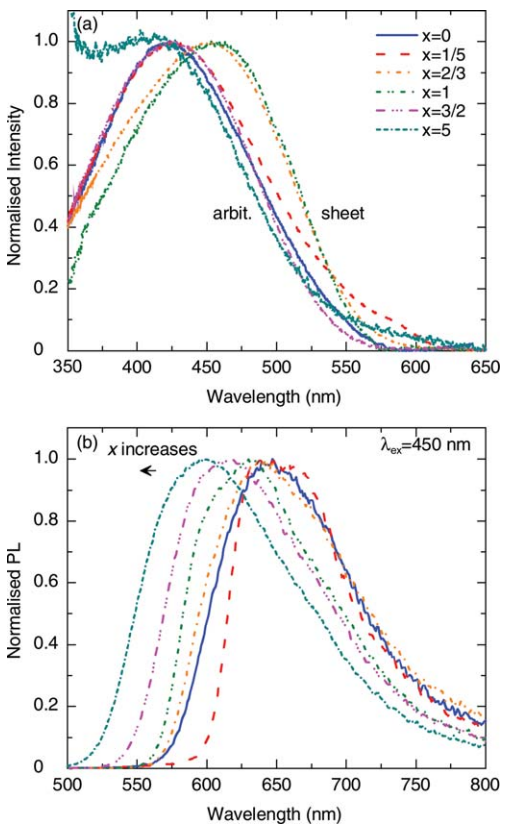

Fig. 9 UV/vis (a) and PL spectra (b) of P3ImiHT–D$_2$O (solid blue lines) and P3ImiHT(SDS)$_x$–D$_2$O x = 1/5 (dashed red lines), x = 2/3 (dashed and dotted orange lines), x = 1 (dashed and double dotted green lines), x = 3/2 (dashed and triple dotted magenta lines) for x = 5 (double dashed and dotted cyan lines). λ_{ex} for PL was 450 nm. The overall concentration of all samples was ~10 mg mL^{-1}.

The PL spectra obtained with λ_{ex} = 450 nm are generally dominated by a broad featureless emission band (Fig. 9b). With the exception between x = 0 and x = 1/5 (showing a slight red-shift), the PL maximum is gradually blue-shifted from 643 nm to 597 nm on increasing the SDS molar fraction from x = 0 to x = 5. This suggests that polymer–polymer interactions are diminished with increasing x and this does not stop at the supposed full complexation point (*i.e.*, at x = 1). An identical trend is observed on excitation at 500 nm, with a slight structuring of the emission spectrum obtained only for x = 1/5 (ESI†).

The "surfactochromic" effect shown in Fig. 9 is seemingly similar to that observed for P3TMAHT(SDS)$_x$–D$_2$O.[40] There are, however, two distinct differences. (i) The peak shift in both directions is significantly reduced for P3ImiHT(SDS)$_x$–D$_2$O, which is observed as a reduced range of spectral colour variation. (ii) In contrast to P3TMAHT(SDS)$_x$–D$_2$O, the vibronic structure formation is generally absent for P3ImiHT(SDS)$_x$–D$_2$O. Generally, surfactant addition can decrease polymer–polymer stacking interactions.

The sample with x = 1/5 appears to be slightly different, which may be due to the formation of ordered ground-state aggregates mediated by polymer–surfactant interactions. These ordered structures deaggregate during further surfactant addition. The SANS data indicate that the polymer remains as a compact particle intertwined with SDS for this sample. It may be that the local order is increased compared to the pure polymer in D$_2$O solution. Note that the interparticle order seen for x = 5 occurs on a completely different length scale (tens of nanometers) without a direct relation to the conformation of single poly-electrolyte chains.

Fig. 10 shows the photoexcitation spectra of P3ImiHT–D$_2$O and P3ImiHT(SDS)$_x$–D$_2$O detected at an emission wavelength (λ_{em}) of 620 nm. These spectra are also broad and featureless and

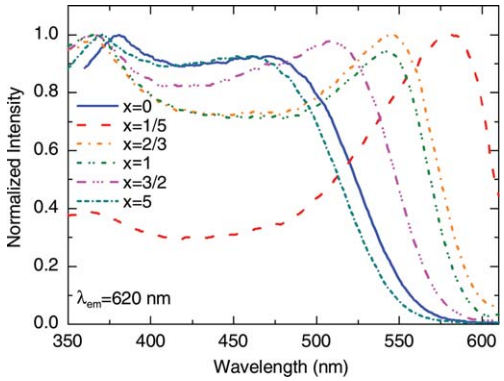

Fig. 10 Photoexcitation spectra of P3ImiHT–D_2O (solid blue line) and P3ImiHT(SDS)$_x$–D_2O $x = 1/5$ (dashed red line), $x = 2/3$ (dashed and dotted orange line), $x = 1$ (dashed and double dotted green line), $x = 3/2$ (dashed and triple dotted magenta line) for $x = 5$ (double dashed and dotted cyan line). The emission wavelength was 620 nm. The overall concentration of all samples was ~10 mg mL^{-1}.

undergo peak maxima variations similar to those observed for the UV/vis absorption spectra, the peak first red-shifting and then progressively blue-shifting with increasing x. When SDS is present in charge excess ($x = 5$), the peak maximum is once again blue-shifted compared to the surfactant free sample ($x = 0$). However, compared to the UV/vis absorption spectra, the excitation spectra are considerably red-shifted (~50 nm) regardless of x. The data are similar for detection at several wavelengths $\lambda_{em} = 580$ nm, 620 nm or 680 nm (ESI†) pointing to a wavelength independence of the excitation spectra and only one kind of emitting species.

The red-shift in the excitation spectrum maxima may be understood in terms of a down-hill energy transfer within the density of states after initial photoexcitation. For most π-conjugated polymers the perfect 1-dimensional π-conjugated molecular wire model is the exception rather than the rule. Structural disorder caused by kinks or twists in the chain typically leads to an inhomogeneous distribution of conformational sub-units with distinct conjugation lengths.[51,52] Excitation into the blue-edge of the absorption spectrum leads mainly to excitation of short (high-energy) segments, which is followed by rapid (sub-picosecond) unidirectional energy migration to longer, low-energy segments. The consequence of this is that essentially all excitation energy is channelled down through the density of states to the lowest energy emissive state regardless of the excitation wavelength.[51,53] The ~50 nm red-shift in the excitation spectra compared to the absorption spectra may therefore be understood in terms of this phenomenon and also reflects the fundamental difference in the electronic transitions measured by the two techniques (excited- and ground-state, respectively).

The variation in the polymer concentration between samples in the P3ImiHT(SDS)$_x$ system must also be mentioned. To maintain a constant concentration of 10 mg mL^{-1} across all samples, the relative P3ImiHT and SDS weight fractions are varied (Table 1). Thus, the sample $x = 5$ is that with the highest SDS concentration, but also the lowest P3ImiHT concentration. π-Stacking interactions are expected to be concentration-dependent, and as such, the decreased polymer concentration, in combination with the additional screening provided by the SDS on increasing x may lead to the observed blue-shift in the photoluminescence.

The maximum red-shift for $x = 1/5$ may be related to the fact that in this case the SDS concentration in the ternary P3ImiHT (SDS)$_x$–D_2O system is below the nominal cmc of the binary SDS–D_2O system (Table 1). Thus, the surfactant may drive local polymer–polymer associations, as seen by disappearing interference maximum in SANS data. In order to study this scenario, we diluted all the samples by a factor of 1000 and repeated the optical spectroscopy measurements expecting reduced interchain interactions. Also, while free SDS micelles are likely to be present for the concentrated samples with $x \geq 2$, where the concentration of nominal excess SDS exceeds the cmc in the binary SDS–D_2O system, no free micelles are expected for any of these diluted samples. The data are shown in ESI†.

Similar, but not identical, surfactochromic trends are observed in the UV/vis absorption and photoexcitation spectra on dilution of the samples to a concentration of 0.01 mg mL^{-1}. The data of P3ImiHT–D_2O are essentially concentration independent. The red-edge shoulder of the photoexcitation spectra for $x = 1/5$ becomes more pronounced upon dilution. On increasing the SDS mole fraction to $x = 1$, the absorption maximum is red-shifted to 457 nm and then blue-shifted back to 445 nm on increasing to $x = 5$ and both spectra exhibit a shoulder on the high-energy side of the absorption band, which becomes more pronounced for $x = 5$. The absence of a complete reversal of the surfactochromic shift back to the blue on increasing x is explained by the absence of SDS micelles.

The PL spectra are concentration dependent and the spectra of diluted samples are considerably blue-shifted compared to their concentrated counterparts. This is not surprising, since polymer–polymer interactions should be reduced on dilution. However, since this effect is far less apparent in the absorption spectra, it suggests that polymer–polymer interactions are preferably documented in the PL spectra as a result of energy transfer processes after photoexcitation. Increasing the SDS molar fraction from $x = 1/5$ to 5 results in increased structuring of the emission bands.

Conclusions

We report on the synthesis of the polymer P3ImiHT and the structural development and subsequent optical changes of P3ImiHT(SDS)$_x$–D_2O with increasing SDS fraction, x. At room temperature, the observed phase transitions are from charged P3ImiHT aggregates with interparticle order to ellipsoidal ($x = 1/5$) and sheet-like P3ImiHT(SDS) particles ($x = 1/2$–1). For $x > 1$, the system is suggested to consist of both P3ImiHT(SDS) aggregates and SDS rich micelles. The polymer conformation within the particles changes correspondingly changing from coils ($x = 1/5$) to polymer sheets ($x = 1$). Strong mutual ordering with a periodicity of 27 nm is seen for $x = 5$. This may be related to the lamellar interparticle order. These transitions are accompanied by surfactochromic changes, visibly observable as solution colour transitions from orange/brown ($x = 0$–1/5) to red/orange ($x = 2/3$–1), orange/brown ($x = 3/2$) and yellow/orange ($x = 5$). P3ImiHT has clear analogies with the previously reported P3TMAHT containing 6-trimethylammoniumhexyl side chains. However, unlike in the case of P3TMAHT, significant

precipitation at the charge compensation point is not observed for P3ImiHT(SDS), which can be attributed to the increased polarity due to the reduced shielding of the ionic centres by the *N*-methylimidazole substituent. Moreover, the spectral shifts are less pronounced for P3ImiHT(SDS). Vibronic structure of the photoabsorption and PL spectra is absent for generally all x. The photophysical characteristics of P3ImiHT(SDS)$_x$–D_2O are best understood in terms of increased or reduced ground-state π–π interactions during SDS addition. The observed effects reflect changes of chain conformation and packing *within* polymer–surfactant aggregates on varying the surfactant fraction, and show that it is possible to modulate the behaviour of CPEs through changes in their ionic head groups. This phenomenon may have important implications in solution processing for organic electronics.

Acknowledgements

This research project has been supported by the European Commission under the 7th Framework Programmes through the 'Research Infrastructures' action of the 'Capacities Programme' Contact No: CP-CSA_INFRA-2008-1.1.1 Number 226507-NMI3.

References

1 A. O. Patil, Y. Ikenoue, F. Wudl and A. J. Heeger, *J. Am. Chem. Soc.*, 1987, **109**, 1858–1859.
2 T. Kawase, T. Shimoda, C. Newsome, H. Sirringhaus and R. H. Friend, *Thin Solid Films*, 2003, **438**, 279–287.
3 E. Tekin, P. J. Smith and U. S. Schubert, *Soft Matter*, 2008, **4**, 703–713.
4 J. L. Lutkenhaus and P. T. Hammond, *Soft Matter*, 2007, **3**, 804–816.
5 L. Zhai and R. D. McCullough, *Adv. Mater.*, 2002, **14**, 901–905.
6 A. Bolognesi, G. Bajo, Z. Geng, W. Porzio and F. Speroni, *Thin Solid Films*, 1994, **243**, 683–686.
7 N. Reitzel, D. R. Greve, K. Kjaer, P. B. Howes, M. Jayaraman, S. Savoy, R. D. McCullough, J. T. McDevitt and T. Bjørnholm, *J. Am. Chem. Soc.*, 2000, **122**, 5788–5800.
8 W. B. Stockton and M. F. Rubner, *Macromolecules*, 1997, **30**, 2717–2725.
9 C. V. Hoven, A. Garcia, G. C. Bazan and T.-Q. Nguyen, *Adv. Mater.*, 2008, **20**, 3793–3810.
10 W.-L. Ma, P. K. Iyer, X. Gong, B. Liu, D. Moses, G. C. Bazan and A. J. Heeger, *Adv. Mater.*, 2005, **17**, 274–277.
11 D. T. McQuade, A. E. Pullen and T. M. Swager, *Chem. Rev.*, 2000, **100**, 2537–2574.
12 S. W. Thomas, III, G. D. Joly and T. M. Swager, *Chem. Rev.*, 2007, **107**, 1339–1386.
13 H. A. Al Attar and A. P. Monkman, *J. Phys. Chem. B*, 2007, **111**, 12418–12426.
14 B. S. Gaylord, A. J. Heeger and G. C. Bazan, *Proc. Natl. Acad. Sci. U. S. A.*, 2002, **99**, 10954–10957.
15 M. Surin, P. G. A. Janssen, R. Lazzaroni, P. Leclere, E. W. Meijer and A. P. H. J. Schenning, *Adv. Mater.*, 2009, **21**, 1126–1130.
16 J. H. Wosnick, C. M. Mello and T. M. Swager, *J. Am. Chem. Soc.*, 2005, **127**, 3400–3405.
17 H. Jiang, P. Taranekar, J. R. Reynolds and K. S. Schanze, *Angew. Chem., Int. Ed.*, 2009, **48**, 4300–4316.
18 G. D. Joly, L. Geiger, S. E. Kooi and T. M. Swager, *Macromolecules*, 2006, **39**, 7175–7177.
19 H. D. Burrows, M. J. Tapia, S. M. Fonseca, A. J. M. Valente, V. M. M. Lobo, L. L. G. Justino, S. Qiu, S. Pradhan, U. Scherf, N. Chattopadhyay, M. Knaapila and V. M. Garamus, *ACS Appl. Mater. Interfaces*, 2009, **1**, 864–874.
20 T. Wågberg, B. Liu, G. Orädd, B. Eliasson and L. Edman, *Eur. Polym. J.*, 2009, **45**, 3228–3233.
21 H.-P. Wang, P. Lu, B.-L. Wang, S. Qiu, M.-R. Liu, M. Hanif, G. Cheng, S.-Y. Liu and Y.-G. Ma, *Macromol. Rapid Commun.*, 2007, **28**, 1645–1650.
22 G. A. Becht, S. Lee, S. Seifert and M. A. Firestone, *J. Phys. Chem. B*, 2010, **114**, 14703–14711.
23 C. T. Burns, S. Lee, S. Seifert and M. A. Firestone, *Polym. Adv. Technol.*, 2008, **19**, 1369–1382.
24 B. Dong, Y. A. Gao, Y. J. Su, L. Q. Zheng, J. K. Xu and Y. Inoue, *J. Phys. Chem. B*, 2010, **114**, 340–348.
25 S.-C. Liao, C.-S. Lai, D.-D. Yeh, M. H. Rahman, C.-S. Hsu, H.-L. Chen and S.-A. Chen, *React. Funct. Polym.*, 2009, **69**, 498–506.
26 X. Crispin, F. L. E. Jakobsson, A. Crispin, P. C. M. Grim, P. Andersson, A. Volodin, C. van Haesendonck, M. Van der Auweraer, W. R. Salaneck and M. Berggren, *Chem. Mater.*, 2006, **18**, 4354–4360.
27 E. H. A. Beckers, P. Jonkheijm, A. P. H. J. Schenning, S. C. J. Meskers and R. A. J. Janssen, *ChemPhysChem*, 2005, **6**, 2029–2031.
28 H. D. Burrows, V. M. M. Lobo, J. Pina, M. L. Ramos, J. S. de Melo, A. J. M. Valente, M. J. Tapia, S. Pradhan and U. Scherf, *Macromolecules*, 2004, **37**, 7425–7427.
29 W. N. George, M. Giles, I. McCulloch, J. S. de Mello and J. H. G. Steinke, *Soft Matter*, 2007, **3**, 1381–1387.
30 M. Knaapila, L. Almásy, V. M. Garamus, C. Pearson, S. Pradhan, M. C. Petty, U. Scherf, H. D. Burrows and A. P. Monkman, *J. Phys. Chem. B*, 2006, **110**, 10248–10257.
31 J. J. Lavigne, D. L. Broughton, J. N. Wilson, B. Erdogan and U. H. F. Bunz, *Macromolecules*, 2003, **36**, 7409–7412.
32 R. D. McCullough and P. C. Ewbank, *Synth. Met.*, 1997, **84**, 311–312.
33 R. D. McCullough, P. C. Ewbank and R. S. Loewe, *J. Am. Chem. Soc.*, 1997, **119**, 633–634.
34 L.-H. Chen, S. Xu, D. McBranch and D. Whitten, *J. Am. Chem. Soc.*, 2000, **122**, 9302–9303.
35 K. Tashiro, K. Ono, Y. Minagawa, M. Kobayashi, T. Kawai and K. Yoshino, *J. Polym. Sci., Part B: Polym. Phys.*, 1991, **29**, 1223–1233.
36 M. J. Winokur, D. Spiegel, Y. Kim, S. Hotta and A. J. Heeger, *Synth. Met.*, 1989, **28**, C419–C426.
37 F. Li, A. A. Martens, A. Aslund, P. Konradsson, F. A. de Wolf, M. A. C. Stuart, E. J. R. Sudhölter, A. T. M. Marcelis and F. A. M. Leermakers, *Soft Matter*, 2009, **5**, 1668–1673.
38 U. Scherf, A. Gutacker and N. Koenen, *Acc. Chem. Res.*, 2008, **41**, 1086–1097.
39 A. Gutacker, S. Adamczyk, A. Helfer, L. E. Garner, R. C. Evans, S. M. Fonseca, M. Knaapila, G. C. Bazan, H. D. Burrows and U. Scherf, *J. Mater. Chem.*, 2010, **20**, 1423–1430.
40 M. Knaapila, R. C. Evans, V. M. Garamus, L. Almásy, N. K. Székely, A. Gutacker, U. Scherf and H. D. Burrows, *Langmuir*, 2010, **26**, 15634–15643.
41 D. Bondarev, J. Zedník, I. Šloufová, A. Sharf, M. Procházka, J. Pfleger and J. Vohlídal, *J. Polym. Sci., Part A: Polym. Chem.*, 2010, **48**, 3073–3081.
42 L. Rosta, *Appl. Phys. A: Mater. Sci. Process.*, 2002, **74**, S52–S54.
43 H. B. Stuhrmann, N. Burkhardt, G. Dietrich, R. Jünemann, W. Meerwinck, M. Schmitt, J. Wadzack, R. Willumeit, J. Zhao and K. H. Nierhaus, *Nucl. Instrum. Methods Phys. Res., Sect. A*, 1995, **356**, 124–132.
44 D. I. Svergun, *J. Appl. Crystallogr.*, 1992, **25**, 495–503.
45 A. K. Morén and A. Khan, *Langmuir*, 1995, **11**, 3636–3643.
46 T. J. Prosa, M. J. Winokur, J. Moulton, P. Smith and A. J. Heeger, *Macromolecules*, 1992, **25**, 4364–4372.
47 T. Zemb and P. Charpin, *J. Phys.*, 1985, **46**, 249–256.
48 P. Mukerjee and K. J. Mysels, *Critical Micelle Concentration of Aqueous Surfactant Systems*, National Bureau of Standards, Washington, DC, 1970.
49 J. Merta, V. M. Garamus, R. Willumeit and P. Stenius, *Langmuir*, 2002, **18**, 7272–7278.
50 P. A. Hassan, S. R. Raghavan and E. W. Kaler, *Langmuir*, 2002, **18**, 2543–2548.
51 H. Bässler and B. Schweitzer, *Acc. Chem. Res.*, 1999, **32**, 173–182.
52 I. Hwang and G. D. Scholes, *Chem. Mater.*, 2011, **23**, 610–620.
53 S. Heun, R. F. Mahrt, A. Greiner, U. Lemmer, H. Bässler, D. A. Halliday, D. D. C. Bradley, P. L. Burn and A. B. Holmes, *J. Phys.: Condens. Matter*, 1993, **5**, 247–260.

